

JEDI: Latent End-to-end Diffusion Mitigates Agent-Human Performance Asymmetry in Model-Based Reinforcement Learning

Jing Yu Lim Zarif Ikram Samson Yu Haozhe Ma Tze-Yun Leong Dianbo Liu

{jy_lim, leongty}@comp.nus.edu.sg, zikram@usc.edu, {samson.yu, haozhe.ma}@u.nus.edu.sg
dianbo@nus.edu.sg

Abstract

Recent advances in model-based reinforcement learning (MBRL) have achieved super-human level performance on the Atari100k benchmark, driven by reinforcement learning agents trained on powerful diffusion world models. However, we identify that the current aggregates mask a major performance asymmetry: MBRL agents dramatically outperform humans in some tasks despite drastically underperforming in others, with the former inflating the aggregate metrics. This is especially pronounced in pixel-based agents trained with diffusion world models. In this work, we address the pronounced asymmetry observed in pixel-based agents as an initial attempt to reverse the worrying upward trend observed in them. We address the problematic aggregates by delineating all tasks as Agent-Optimal or Human-Optimal and advocate for equal importance on metrics from both sets. Next, we hypothesize this pronounced asymmetry is due to the lack of temporally-structured latent space trained with the World Model objective in pixel-based methods. Lastly, to address this issue, we propose Joint Embedding Diffusion (JEDI), a novel latent diffusion world model trained end-to-end with the self-consistency objective. JEDI outperforms SOTA models in human-optimal tasks while staying competitive across the Atari100k benchmark, and runs 3 times faster with 43% lower memory than the latest pixel-based diffusion baseline. Overall, our work rethinks what it truly means to cross human-level performance in Atari100k.

1 Introduction

Model-based reinforcement learning (MBRL) uses *world models* [70, 25] of environmental dynamics to enhance decision-making efficiency and performance in sequential decision tasks. Unlike model-free approaches that directly approximate value functions or policies from interactions, MBRL learns an internal representation of the environment to anticipate outcomes and plan ahead. This enables the agent to plan and reason ahead, improving sample efficiency and adaptability in complex or partially observable environments [27, 28, 75, 29].

The principle accompanying MBRL is rooted in broader theories of intelligence. For example, Ma et al. [47] asserts *parsimony* and *self-consistency* as foundational for the emergence of intelligence—a view shared by LeCun [41] and aligned with the *Free Energy Principle* [21, 20], which argues that intelligence emerges from surprise minimization between internal predictions and observations. In the MBRL paradigm, as shown in Hafner et al. [27], parsimony is achieved by compression from high-dimensional image to low-dimensional latent space using the encoder, while self-consistency is achieved through the next-state prediction objective of the world model [26, 27, 30]. This setup forms a highly coupled feedback loop with an RL agent: the world model improves by maximizing

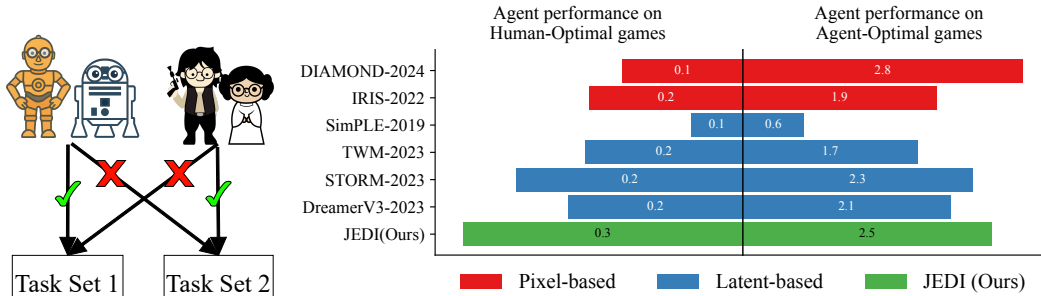


Figure 1: *Left*: Performance asymmetry on RL tasks. Tasks where humans excel often differ from where RL agents excel—often due to reward hacking or representation learning failures [65, 24]. *Right*: MBRL agents exhibit a large performance asymmetry between Human-Optimal and Agent-optimal tasks, often outperforming in the latter by over an order of magnitude. This disparity is especially pronounced in pixel-based MBRL agents.

self-consistency between its predictions and real data, while the RL agent improves its policy by training on the imagined latent rollouts, which in turn leads to more informative data collection.

This paradigm is effective, recently crossing the human-level performance on the challenging Atari100k benchmark [38], which limits the agent to 100K environment steps or around 2 hours of human game play [48, 59, 29, 79]. This marks a stark contrast to pre-existing benchmarks with tens to hundreds of million environment steps primarily tackled by model-free RL [11].

The crossing of human-level performance is a notable milestone. When [50] crossed the barrier in 2015, it scored close to a professional game tester on the majority of the tasks, sparking a deep RL revolution that led to breakthroughs like [63, 64]. However, we discover that *crossing human-level performance* with MBRL is not as conclusive as before and even problematic. For example, the recent top-performing approach uses a diffusion model [67, 34] for its conditional distribution modeling and high-fidelity image generation [60, 17, 33], enabling pixel-perfect rollout that a pixel-based RL agent trains on, driving its state-of-the-art (SOTA) performance [4]. Yet, these models may overfit *some* benchmark metric rather than *match* human-performance.

In particular, we observe a striking asymmetry in MBRL performance across the 26 tasks. While the mean human normalized score (HNS) [11] suggests super-human performance, a closer look reveals that MBRL agents *massively* outperform humans in tasks humans perform poorly—what we call *agent-optimal tasks*—and fail in tasks where human players excel—*human-optimal tasks* [48, 59, 29, 79, 4].¹

We illustrate this in Figure 1: MBRL algorithms, especially those directly operating on the pixel-space, underperform dramatically in human-optimal tasks. As a result, averaging HNS can be misleading—a handful of *inflated* scores on the agent-optimal tasks compensate for regressing scores on human-optimal tasks that barely contribute anything to the *SOTA* score [4]. This raises a critical question: *have we really crossed the human-level performance, or are we just chasing metric artifacts?*²

In this work, we limit our scope to address the pronounced asymmetry observed in pixel-based agents to reverse the worrying trend of increasing performance asymmetry in pixel-based agents across time (Fig 1). First, we show the performance asymmetry of RL agents among Atari100k tasks, categorize them as either Agent-Optimal or Human-Optimal, and advocate for equal emphasis on evaluation metrics across both categories. Next, we hypothesize this pronounced asymmetry arises from training diffusion based world models detached from its RL agent’s encoder. This neglects the self-consistent representation learning we discussed above and sacrifices action temporal reasoning necessary in many tasks. As the field rapidly shifts towards training large latent diffusion world models with fixed, pre-trained encoder lacking self-consistent representations [60], performance asymmetry is likely to worsen, especially for agents trained in such temporally unstructured latent space [44, 55, 2].

¹We define the sets of agent-optimal tasks and human-optimal tasks consisting of 13 tasks each in §5.1.

²Observant readers may connect this phenomena to the Moravec’s paradox [52, 51]. Regrettably, this is far beyond the scope of this text.

To address this issue, we propose the **Joint Embedding Diffusion (JEDI)** world model—a latent, end-to-end diffusion-based world model trained with a self-consistency objective inspired by Joint Embedding Predictive Architecture (JEPA) [6]. By combining the visual modeling power of diffusion models with the action temporal reasoning capabilities of latent world models, JEDI bridges the gap across both types of tasks. To the best of our knowledge, JEDI is the first framework that enables search-free, reconstruction-free latent representation prediction directly from the diffusion model’s denoising inference—without using hidden state extraction, noised input, distillation, or train-time iterative denoising. This is also the first work that shows that diffusion is compatible with JEPA—challenging prevailing beliefs that JEPA requires bespoke loss functions [22, 13, 73, 6, 9]—which enables JEDI to capture temporally-structured representation without recurrent architectures [18, 35]. On Atari100k, JEDI yields SOTA performance on human-optimal tasks and remains competitive across the full benchmark—while enjoying **3× faster inference, 2× training, and requiring only 57% GPU memory** compared to the SOTA diffusion-based world model [4].

In summary, our contributions are following.

1. We identify a significant performance asymmetry in MBRL agents across different tasks relative to human performance (§1) and propose a solution to the current problematic aggregates masking underlying biases (§5.1).
2. We propose a hypothesis linking the pronounced performance asymmetry in pixel-based agents to the absence of self-consistent representation learning (§3).
3. We propose JEDI, a latent end-to-end diffusion-based world model with a self-consistency objective to mitigate this asymmetry and bring us closer to holistic human level performance. (§4). We validate our method empirically and qualitatively (§5, §5.3).

2 Background and Related Work

2.1 Joint Embedding Prediction Architecture (JEPA)

JEPA is a non-contrastive Self-Supervised Learning (SSL) representation learning framework first formalized by [23]. It learns by training a predictor to map target embeddings of equivariant views of data modality in the same latent space. To avoid representation collapse—a problem that occurs when a representation learner tends to represent data with similar embeddings, modern day JEPA generally relies on data augmentation and self teacher-student training [13], which is a result of a number of works. Grill et al. [22] originally proposed the use of a symmetric L_2 loss and hypothesized that it allows for representation collapse to be an unstable solution. Caron et al. [13] proposed cross-entropy loss with the target centered with a moving average and sharpened with a low temperature softmax. Assran et al. [6] replaced the view-invariance of images with patch-wise prediction and used L_2 loss. Bardes et al. [9] proposed the use of L_1 loss, connecting this to the minimization of deviation from the Mean Absolute Median. Our work shows that JEPA training paradigm is directly compatible with the diffusion loss as introduced by [39].

2.2 Model-Based Reinforcement Learning

MBRL attempts to solve Partially Observable Markov Decision Processes (POMDP) environments [37] with RL where the agent does not have direct access to states, z_t , and only have access to observations containing partial information o_t . The objective is to maximize the expected cumulative sum of discounted rewards. This is typically done through learning a generative world model which consists of an encoder, dynamics model, reward and termination model with SSL. The RL agent is then learned within compressed latent trajectories of the world model, and the trained agent is deployed in the real environment to collect data for training the world model, and the cycle repeats.

Related works. One of the earliest work involving world models can be attributed to Dyna [70] that uses model imagination to augment policy learning. With improvements in deep learning came [25] where the authors proposed learning the world model in the pixel space. Concurrently, [26] proposed learning a world model and using it for planning with model predictive control (MPC), becoming one of earliest works to successfully use world modeling on the DeepMind Visual Control (DMC) tasks [71]. With the success of [26] came the Dreamer [27–29]. Dreamer [27] learns an actor-critic network using the representations learnt by an end-to-end trained world model. DreamerV2 [28] improves the representations by replacing the Gaussian latents with reparameterized gradients [40]

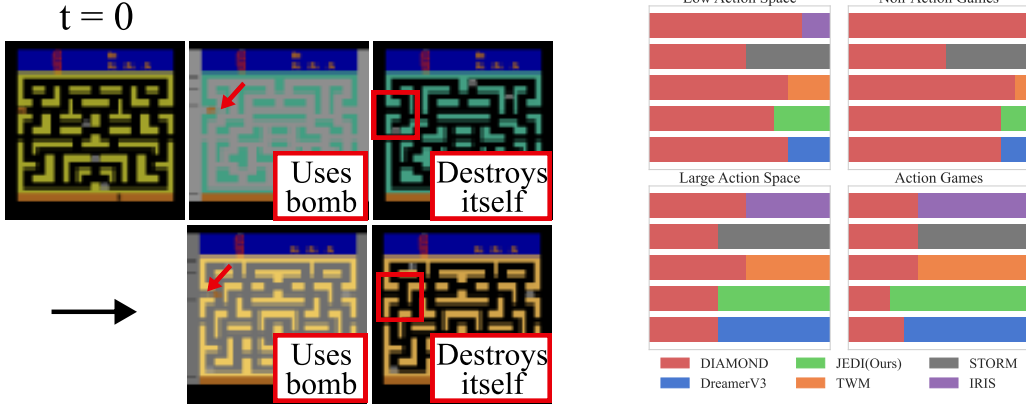


Figure 2: *Left*: Example trajectory of DIAMOND on *BankHeist* displays self-sabotaging behaviour as it is unable to reason about its high complexity action space. *Right*: DIAMOND vs. other agents in different environment settings. DIAMOND’s performance bias towards Non-Action environments with Low Action Space.

with straight-through gradients [12]. DreamerV3 [29] offers architectural improvements to address scaling challenges in world models for generalizing across multiple domains. Parallely, transformer based world models have been developed, with IRIS [49] developing a GPT-like world model with discretized pixel observation tokens as its input. Besides, multiple work has been proposed that uses transformer-based backbone while retaining similarity to Dreamer-based world models, such as STORM [79], TransDreamer [14], and TWM [59]. Hansen et al. [30, 31] introduced the use of JEPA for learning world model dynamics and differs from us as they use an MLP as the world model.

3 Performance asymmetry in pixel-based MBRL

As discussed in §1, pixel-based agents show pronounced asymmetry when compared to humans. We hypothesize that this pronounced bias arises from a lack of a structured prior: unlike agents that learns its policy under states learnt with a world model’s compressed next state, reward, and termination prediction objective, pixel-based agent must learn its own latent space through only temporal-difference (TD) updates [69]. This leads to brittle, reactive policies that excel in reward-hackable environments. To see how, take, for example, the game *BankHeist* presented in Figure 7. Here, an agent earns immediate rewards by robbing banks and can eliminate enemies—or itself—using a bomb action. A superficially effective yet ultimately brittle strategy would be to reward hack by moving between maps in quick succession and robbing banks that spawn near the exit for easy points. DIAMOND, a SOTA pixel-based agent, discovers this reward-hacking behavior (*left* of Figure 2), but it remains unstable—it wanders aimlessly and ultimately bombs itself.

Crucially, this is *not* how humans think. Humans prioritize structured, temporally informed behavior—avoiding high-risk actions and applying long-term reasoning over low-level reward exploits.

To better study this mismatch, we analyze environment factors that closely relates with pixel-based agents performance. Two features standout the most.

Action-oriented dynamics. In tasks where the environment rewards the agent for neutralizing an enemy—we call *action games*—the agent has to apply long-term reasoning against the dynamic decisions taken by the enemy.

Action-space complexity. Tasks with larger action-space favors high-dexterity of humans: without temporal reasoning, an agent struggles in such tasks.

As we show in Figure 2 (*right*), pixel-based agents such as DIAMOND excel in non-action games with low action-space, while they struggle in games that reward temporal reasoning. This trend suggests a bias of current pixel-based MBRL agents towards short-term reactivity, constructing the pronounced asymmetry compared to humans. These findings motivate us to build an agent that retains

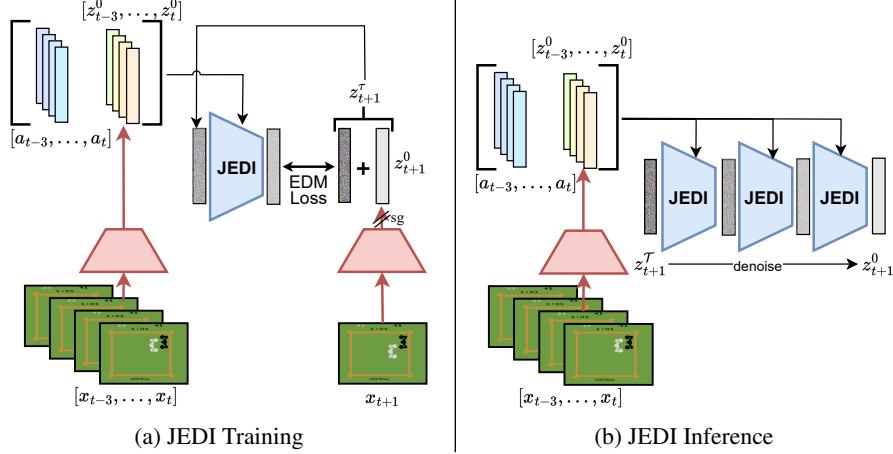


Figure 3: Joint Embedding Diffusion (JEDI) World Model. (a) During training, the current image observations $[x_{t-3}, \dots, x_t]$ is passed through the world model encoder to derive the low dimensional latent states $[z_{t-3}^0, \dots, z_t^0]$ and it is passed into the diffusion model together with the actions as the conditioning. The target next state z_{t+1}^τ is derived from passing x_{t+1} through the same encoder, except with stop-gradient. A noise is sampled and scaled according to the sampled diffusion time step τ , and this is passed to the diffusion model as input. Given these, the diffusion model learns to predict the direction towards the next state, training both the encoder and diffusion model in an end-to-end fashion. (b) During inference, the same conditioning is derived and passed into the diffusion model. A random noise is sampled and passed into diffusion model as input. Given these, the model predicts the direction towards the next state and iteratively denoise to arrive at the clean next state.

the expressiveness and modeling capabilities of DIAMOND, yet incorporates a latent space that is learnt end-to-end. In the next section, we will show how we achieve this.

4 JEDI: World Model with latent end-to-end diffusion

To address the agent-human performance asymmetry, we introduce Joint Embedding Diffusion World Model (JEDI) as shown in Figure 3. During JEDI training (Fig 3a), the encoder first derives the latent states from observations. Second, the current set of latent states and actions are passed to the diffusion model as conditioning. The input is the next time step latent state without gradients added to the sampled noise scaled according to the sampled diffusion time step. With these, the diffusion model regresses towards the direction of the next latent state. During inference (Fig 3b), the conditioning is derived in the same manner, and the starting input is random noise. With the predicted direction towards the clean latent state, we can iteratively denoise and predict it. Mathematically:

$$\text{World Model: } \begin{cases} \text{Encoder:} & z_t^0 = \mathbf{E}_\phi(x_t), \\ \text{Latent Diffusion Dynamics Model:} & \hat{z}_{t+1}^\tau \sim \mathbf{S}(\mathbf{D}_\theta(\hat{z}_{t+1}^\tau, Z_t^\tau)), \\ \text{Reward \& Termination} & (\hat{r}_t, \hat{d}_t) = \mathbf{R}_\psi(z_t^0), \end{cases} \quad (1)$$

where t is the environment time step, x_t is the original environment observation, \mathbf{E}_ϕ is the encoder with parameter ϕ , z_t^0 refers to the clean latent at environment time step t , $x_t \in [0, 1]^{3 \times 64 \times 64}$ is the environment image input and $z_t \in [-3, 3]^{16 \times 8 \times 8}$ is the latent state. $\tau \in [0, 1] \sim \text{LN}$ is the diffusion time step determining the noise schedule $\sigma(\tau)$ with 0 being clean latent state, LN refers to the logit-normal distribution [39]. \mathbf{D}_θ is the single-step conditioned denoising (or “reverse-diffusion”) operator and \mathbf{S} is the ODE or SDE solver for multi-step denoising inference. $r_t \in \{-1, 0, 1\}$ is the reward and $d_t \in \{0, 1\}$ is the episode termination flag. We follow the pre-conditioning diffusion paradigm as introduced in [39]

$$\mathbf{D}_\theta(z_{t+1}^\tau, Z_t^\tau) = c_{\text{skip}}^\tau z_{t+1}^\tau + c_{\text{out}}^\tau \mathbf{F}_\theta(c_{\text{in}}^\tau z_{t+1}^\tau, Z_t^\tau). \quad (2)$$

where, c_{noise}^τ is a fixed transformation of τ , $Z_t^\tau := (c_{\text{noise}}^\tau, z_{t:t-3}^0, a_{t:t-3})$, and $c_{\text{skip}}^\tau, c_{\text{out}}^\tau, c_{\text{in}}^\tau$ are preconditioning variables depending on sampled noise for better behavior of \mathbf{F}_θ , a neural network.

Joint Embedding Diffusion loss. The loss function of the latent diffusion dynamics model, $\mathcal{L}_{dyn}(\theta, \phi)$ is re-parameterized to:

$$\mathbb{E}_{z_{1:T} \sim q, x_{1:T} \sim p, \tau \sim \text{LN}} \left[\left\| \sum_{t=1}^T \mathbf{F}_{\theta}(c_{\text{in}}^{\tau} \text{sg}(z_{t+1}^{\tau}), Z_t^{\tau}) - \frac{1}{c_{\text{out}}^{\tau}} (\text{sg}(z_{t+1}^0) - c_{\text{skip}}^{\tau} \text{sg}(z_{t+1}^{\tau})) \right\|^2 \right] \quad (3)$$

where $q(z_t) = (\mathbf{E}_{\phi})_{\#} p(x_t)$ is the deterministic push forward mapping of \mathbf{E}_{ϕ} on the randomly sampled x_t and sg refers to stop-grad. Sampling τ from a logit-normal prior LN ensures the middle noise level are visited more often during training.

The Cross-Entropy (CE) loss for the Reward and Termination model is:

$$\mathcal{L}_{r\&d}(\psi, \phi) = \mathbb{E}_{z_{1:T}^0 \sim q, (x_{1:T}, r_{1:T}, d_{1:T}) \sim p} \sum_{t=1}^T \text{CE}(\mathbf{R}_{\psi}(z_t^0), (r_t, d_t)) \quad (4)$$

Crucially, the encoder learns through both 3 and 4 where the gradients flow back to \mathbf{E}_{ϕ} through z_t^0 and **not** the encoded targets, z_{t+1} . This trains the encoder while training the latent diffusion model to predict the next latent representation during inference time without any reconstruction loss.

End-to-end latent space diffusion. On top of using stop-grad to prevent the encoder from learning from the targets, we use a learning rate of 0.3 for the input encoder to prevent representation collapse which was shown to work well in [30, 31]. Conventional image diffusion has a natural clamp during denoising inference as $x_t \in [0, 1]$. To ensure that the denoising process is stable, we impose a differentiable clamp function, $C(z_t^0) = \tanh(z_t^0/s)s$, scaled by a factor, $s = 3$ on the outputs of \mathbf{E}_{ϕ} as well as on \mathbf{D}_{θ} during inference.

Temporally structured latent space. We enable our latent space to be structured for capturing near-term temporal information by placing the single-step prediction of \mathbf{D}_{θ} for each time step with attached gradients as the input to the JEDI loss at the next time step. This enables the gradients from future JEDI loss states to flow back to the encoder. However, this means that \mathbf{E}_{ϕ} only sees the image observations at the starting time steps. Hence, with every batch of trajectory sampled, we randomly switch with uniform probability between using the output of \mathbf{D}_{θ} and \mathbf{E}_{ϕ} for the following time step JEDI loss in order to balance the capturing of near-horizon information and providing sufficient training data to the encoder.

Policy. The actor, $\pi_{\omega}(a_t|z_t)$, and critic, $V_{\omega}(z_t)$, trains after the JEDI world model finishes its current training iteration. We intentionally use REINFORCE [74] policy gradient to train the RL agent as it does not require expensive gradient computation through the multi-step denoising of the JEDI model, and it has been effective on Atari100k [28, 4]. To train the LSTM-based actor-critic network [35], we freeze JEDI world model and rollout latent trajectories. After the policy finishes its current training iteration, its parameters alongside JEDI encoder’s parameters are frozen and both are deployed in the actual environment to collect more data and the cycle continues.

We emphasize that we directly used the implementation of the pixel-based diffusion MBRL agent by Alonso et al. [4] with minimal changes while maintaining the same number of parameters. This is to attribute as much of the emergent difference in performance to JEDI. Refer to appendix for details.

5 Experiments

We begin our evaluation with a systematic investigation of the asymmetry present in the Atari100k benchmark through the lens of fairness research, showing that JEDI bridges the gap between human and agent performance by reducing asymmetry in performance. Then, we present our results on the Atari100k, demonstrating that JEDI compares favorably to SOTA agents while improving its computational efficiency and scalability. Next, we validate our claim qualitatively, showing JEDI shows clever strategies of temporal reasoning compared to its pixel-based counterpart. Finally, we motivate our design choices through thorough ablation studies. For all experiments, we run JEDI on Atari100k [38] across 3 seeds and report the mean scores achieved by the final policy on 100 test episodes. Our experiment runtime is 2 days and memory requirement is 7GB.

For experiments, we compare the original average human scores on Atari100k [38, 56] and pre-existing MBRL agents’ performance. We derive the general agent performance by averaging the HNS of 4 pre-existing MBRL works which hovers around human-level performance [48, 59, 29, 79]. These works are amongst the first MBRL works to reach human-level performance.

5.1 Classification of tasks based on asymmetry

Setup. To study the performance asymmetry between humans and agents, we characterize the general behavior of modern model-based reinforcement learning (MBRL) agents, we compute the average human-normalized score (HNS) across four state-of-the-art MBRL methods that approach or surpass human-level performance: IRIS [48], TWM [59], DreamerV3 [29], and STORM [79]. These agents represent the current frontier of pixel-based MBRL under the 100k interaction constraint. Inspired by prior model-free RL research [50], we adopt a classification scheme that thresholds on the the human normalized score (HNS). Concretely, we define tasks on which averaged agent HNS exceeds 75% as *agent-optimal* and those falling below as *human-optimal*. This classification also provides a balanced set of 13 games per group that we present in Table 1.

Table 1: Agent-Optimal and Human-Optimal Atari100k tasks with HNS.

| Agent-Optimal Tasks | HNS | Human-Optimal Tasks | HNS |
|---------------------|------|-----------------------|-------|
| <i>Boxing</i> | 6.35 | <i>BankHeist</i> | 0.59 |
| <i>Krull</i> | 5.33 | <i>DemonAttack</i> | 0.31 |
| <i>CrazyClimber</i> | 2.52 | <i>Hero</i> | 0.27 |
| <i>Gopher</i> | 1.72 | <i>BattleZone</i> | 0.25 |
| <i>RoadRunner</i> | 1.65 | <i>Frostbite</i> | 0.22 |
| <i>Jamesbond</i> | 1.52 | <i>Qbert</i> | 0.21 |
| <i>Assault</i> | 1.36 | <i>MsPacman</i> | 0.20 |
| <i>Breakout</i> | 1.25 | <i>Asterix</i> | 0.093 |
| <i>KungFuMaster</i> | 1.03 | <i>ChopperCommand</i> | 0.088 |
| <i>Pong</i> | 1.03 | <i>Amidar</i> | 0.085 |
| <i>Kangaroo</i> | 0.85 | <i>Alien</i> | 0.077 |
| <i>UpNDown</i> | 0.78 | <i>PrivateEye</i> | 0.032 |
| <i>Freeway</i> | 0.75 | <i>Seaquest</i> | 0.014 |

Fairness-inspired evaluation. Inspired by fairness research, we adapt the metrics used for *Demographic Parity* [32, 10] for MBRL evaluation. Instead of equal *performance* across two groups, we advocate for equal *importance* across both groups. We define this with the following example.

$$\text{IM}(m_1 \sim \mathbf{P}(M|\text{Agent-Optimal} = \text{True})) = \text{IM}(m_2 \sim \mathbf{P}(M|\text{Human-Optimal} = \text{True})) \quad (5)$$

where M can be any performance metric (e.g., HNS) and IM is a function mapping the sampled m to its importance. As mentioned above, this equation only advocates equal importance, rather than equal performance. We argue that this promotes equitable research, shifts focus from aggregate metrics, and debiases MBRL research from agent-optimal tasks as a result. With this in mind, we show our results over the 2 sets in Table 2.³

Results. Table 2 shows that JEDI achieves SOTA results on the human-optimal sets, outperforming all baselines in mean, median, and interquartile mean (IQM), HNS, and optimality gap, with over twice better result compared to the next-best baseline, DIAMOND. Remarkably, JEDI is the lookahead-free method to achieve super-human performance in *BankHeist* from the human-optimal set. On agent-optimal sets, JEDI retains runner-up performance across all metrics except optimality gap, where it trails by a small margin. Results in our supplementary tables further illustrates this symmetry, where JEDI attains a more even distribution of top results across tasks. The results highlight its balanced performance, bridging the gap between human and agent performance.

Table 2: Aggregate Atari100k performance of all methods. Bold = best, underline = runner-up. Mean, Median, and Interquartile Mean (IQM) is with reference to Human Normalized Scores (\uparrow); Optimality Gap (\downarrow) is the overall gap to human-level performance. DIAMD = DIAMOND, DrmrV3 = DreamerV3. JEDI achieves SOTA results on all metrics in Human-Optimal tasks while achieving runner-up performance on all metrics in Agent-Optimal tasks except optimality gap.

| Agent-Optimal | IRIS | TWM | DrmrV3 | STORM | DIAMD | JEDI | Human-Optimal | IRIS | TWM | DrmrV3 | STORM | DIAMD | JEDI |
|---------------------------------|--------------|-------|--------|-------|--------------|-------|---------------------------------|-------|--------------|--------------|-------|-------|--------------|
| #Superhuman (\uparrow) | 9 | 8 | 9 | 10 | 11 | 9 | #Superhuman (\uparrow) | 1 | 0 | 0 | 0 | 0 | 1 |
| Mean (\uparrow) | 1.930 | 1.746 | 2.071 | 2.293 | 2.791 | 2.470 | Mean (\uparrow) | 0.162 | 0.166 | <u>0.184</u> | 0.162 | 0.127 | 0.295 |
| Median (\uparrow) | 1.226 | 1.119 | 1.356 | N/A | 2.510 | 1.749 | Median (\uparrow) | 0.078 | <u>0.109</u> | 0.106 | N/A | 0.075 | 0.164 |
| IQM (\uparrow) | 1.461 | 1.051 | 1.303 | N/A | 2.150 | 1.631 | IQM (\uparrow) | 0.072 | 0.112 | <u>0.122</u> | N/A | 0.091 | 0.153 |
| Optimality Gap (\downarrow) | <u>0.172</u> | 0.185 | 0.176 | N/A | 0.087 | 0.225 | Optimality Gap (\downarrow) | 0.852 | 0.840 | <u>0.823</u> | N/A | 0.873 | 0.735 |

5.2 Atari100k results

Next, we turn our attention to Atari100k as a whole. Figure 4 demonstrates that we achieve SOTA optimality gap, outperform DIAMOND on median score, and achieve second-best HNS mean across all baselines. Remarkably, we achieve these results with over 2 times faster training, over 3 times faster inference, and around 43% less GPU memory usage compared to DIAMOND (Fig 6). This is solely due to the 12 times compression achieved with JEDI.

³For this very reason, we normalize Figure 1 by the maximum in each subplot to attain the equal length bars.

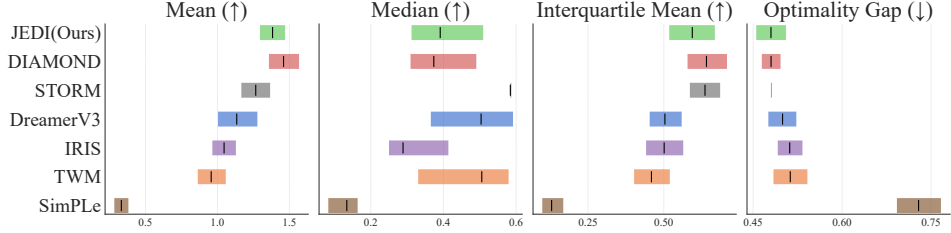


Figure 4: Overall aggregates on Atari100k. Mean, Median, and Interquartile Mean (IQM) is with reference to Human Normalized Scores (\uparrow); Optimality Gap (\downarrow) is the overall gap to human-level performance. JEDI achieves SOTA in optimality gap while achieving runner-up performance in Mean. It outperforms the SOTA pixel-based agent baseline in Median.

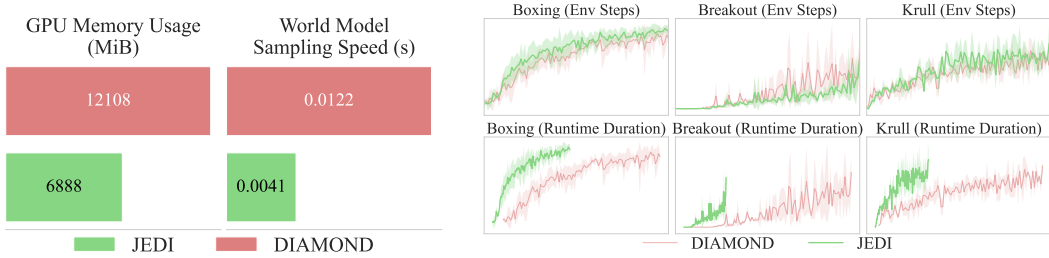


Figure 6: *Left*: JEDI uses 57% of DIAMOND’s GPU Memory Usage while having 3 \times the world model sampling speed. *Right*: Training curves against environment steps (top) and actual runtime duration (bottom). JEDI’s performance matches DIAMOND’s while running 2 \times faster.

We also demonstrate the prowess of JEDI in modelling complex multimodal probability distributions by comparing JEDI and DreamerV3 on 3 Atari100k tasks with stochastic frameskipping uniform between 2 and 6. Our results in Figure 5 shows that we outperform DreamerV3 substantially. Moreover, our algorithm is much more robust to the task-related aleotoric uncertainty introduced as our performance drop is not as significant as the baseline.

5.3 Qualitative validation

We visualize in Figure 7 the differences between the DIAMOND and JEDI policies for 3 tasks: *BankHeist*, *DemonAttack* and *Hero*. These tasks require high action temporal reasoning. In *BankHeist*, the agent robs banks to get immediate rewards and can destroy the enemy and itself by dropping bombs. We discover that a super-human policy was to reward hack by moving between maps in quick succession and robbing banks that spawn near the exit for easy points. The DIAMOND agent learns this, but also wanders aimlessly and destroys itself with the bomb action. JEDI learns the same policy, but the agent moves rapidly between maps and does **not** use the bomb action at all, achieving SOTA performance. We observe similar behaviors in *Hero* where the DIAMOND agent behaves inefficiently (it misses obstacles it means to destroy) and destroys itself more frequently than JEDI. In *DemonAttack*, the DIAMOND agent learns an ineffective policy in which it stays at the same spot and jitters to lure enemies to its spot. This only works on the enemy closest to the agent, leaving it firing at nothing after that enemy has been destroyed. JEDI chases enemies and neutralizes them effectively, achieving higher performance. In all three tasks, the effective policy for consistent

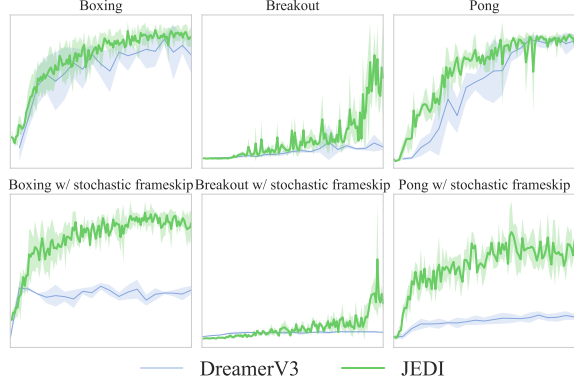


Figure 5: JEDI vs. DreamerV3 in environments with stochastic frame-skipping. JEDI consistently outperform SOTA latent-based agent in all aspects. JEDI’s performance is more robust to high task-related aleotoric uncertainty.

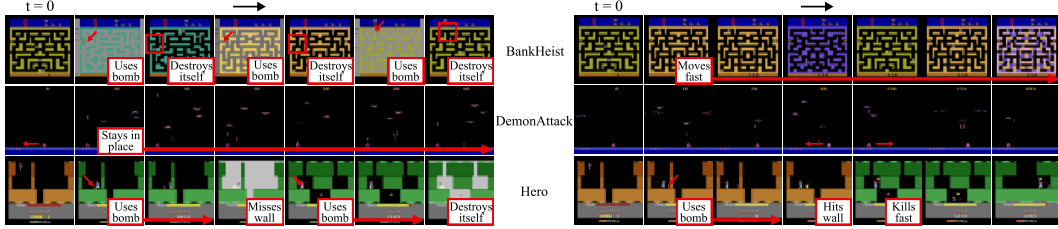


Figure 7: Example trajectories with DIAMOND (left) and JEDI (right) on three tasks. For each game, we show the initial observation at $t = 0$ and six salient frames from a single trajectory. We observe that JEDI is better at temporal causal action reasoning for maximizing short-term rewards. JEDI is more effective at destroying enemies in *DemonAttack* (chasing and shooting them accurately) and obstacles in *Hero* (dropping bombs accurately at walls). In *BankHeist*, both models shuffle between maps to rob banks that spawn at the exit for easy points (i.e. reward hacking). However, JEDI moves much faster and gets more rewards. In both *BankHeist* and *Hero*, JEDI’s effective action choices reduce self-destruction from randomly dropping bombs, delaying early terminations and enabling longer horizons for getting rewards.

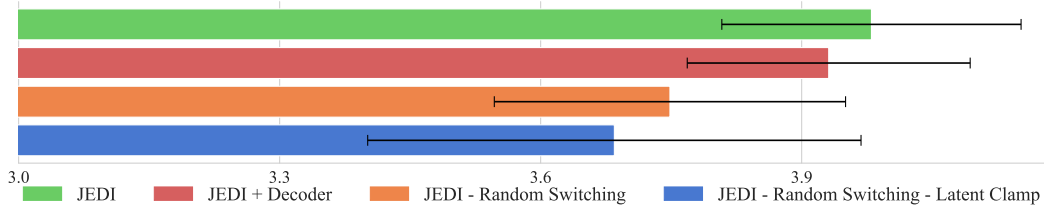


Figure 8: Ablation study. We tested the mechanisms we put in place for effective end-to-end latent diffusion and show that the clamping and random switching is the most effective, outperforming even gradients from decoder reconstruction.

short-term rewards involves destroying enemies or moving quickly (minimizing unnecessary actions that might be self-destructive), and JEDI does these well. Both outcomes reduce early termination, resulting in higher returns. These examples show that the DIAMOND agent is unable to reason well about its actions into the near future, whereas the JEDI agent is able to do so. We believe that this supports our hypothesis of connecting the pronounced performance asymmetry to the lack of a temporally structure latent space provided to DIAMOND.

Key Insight. By causally predicting the next state, reward and termination, given the current state and action, JEDI encoder learns a well-structured latent space for effective causal action reasoning for future rewards. Every additional action adds exponential state-action-reward-termination sequence combinations and the pixel-based agent has to learn a latent state that is well-structured for these combinations from scratch with only the temporal difference learning objective [69].

5.4 Effect of different components

To demonstrate our current design decisions, we conduct an ablation study (Fig 8) on 7 tasks in the Agent-Optimal set with the following ablations : (1) JEDI w/o random switching of \mathbf{E}_ϕ and \mathbf{D}_θ output for following time step JEDI loss and w/o tanh scaled with a factor of 3 on the latent space, (2) JEDI w/o random switching, (3) JEDI w/ reconstruction decoder loss gradients, (4) JEDI.

6 Discussion and limitations

The scope of our work and the definitions proposed is limited to the Atari100k benchmark [38]. Even though JEDI achieves SOTA performance in the Human-Optimal tasks, the performance is still around one order of magnitude smaller than the performance on the Agent-Optimal tasks, indicating a wide gap in performance in these two tasks. Despite our method beating image-based diffusion methods in terms of computation speed, we are slower than existing latent MBRL baselines due to the nature of the multi-step denoising inference with every next state sampled. We are limited by the academic compute budget and hence only conducted the experiments with 3 seeds, and also limited to the small environment steps regime and small set of tasks in Atari100k, as opposed to the larger set of tasks in Atari Benchmark [11].

References

- [1] Korbinian Abstreiter, Sarthak Mittal, Stefan Bauer, Bernhard Schölkopf, and Arash Mehrjou. Diffusion-based representation learning. *arXiv preprint arXiv:2105.14257*, 2021.
- [2] Niket Agarwal, Arslan Ali, Maciej Bala, Yogesh Balaji, Erik Barker, Tiffany Cai, Prithvijit Chattopadhyay, Yongxin Chen, Yin Cui, Yifan Ding, et al. Cosmos world foundation model platform for physical ai. *arXiv preprint arXiv:2501.03575*, 2025.
- [3] Michael S Albergo, Nicholas M Boffi, and Eric Vanden-Eijnden. Stochastic interpolants: A unifying framework for flows and diffusions. *arXiv preprint arXiv:2303.08797*, 2023.
- [4] Eloi Alonso, Adam Jelley, Vincent Micheli, Anssi Kanervisto, Amos Storkey, Tim Pearce, and François Fleuret. Diffusion for world modeling: Visual details matter in atari. *arXiv preprint arXiv:2405.12399*, 2024.
- [5] Brian D.O. Anderson. Reverse-time diffusion equation models. *Stochastic Processes and their Applications*, 12(3):313–326, 1982. ISSN 0304-4149. doi: [https://doi.org/10.1016/0304-4149\(82\)90051-5](https://doi.org/10.1016/0304-4149(82)90051-5). URL <https://www.sciencedirect.com/science/article/pii/0304414982900515>.
- [6] Mahmoud Assran, Quentin Duval, Ishan Misra, Piotr Bojanowski, Pascal Vincent, Michael Rabbat, Yann LeCun, and Nicolas Ballas. Self-supervised learning from images with a joint-embedding predictive architecture. In *Proceedings of the IEEE/CVF Conference on Computer Vision and Pattern Recognition*, pages 15619–15629, 2023.
- [7] Omer Bar-Tal, Hila Chefer, Omer Tov, Charles Herrmann, Roni Paiss, Shiran Zada, Ariel Ephrat, Junhwa Hur, Guanghui Liu, Amit Raj, et al. Lumiere: A space-time diffusion model for video generation. In *SIGGRAPH Asia 2024 Conference Papers*, pages 1–11, 2024.
- [8] Dmitry Baranchuk, Ivan Rubachev, Andrey Voynov, Valentin Khrulkov, and Artem Babenko. Label-efficient semantic segmentation with diffusion models. *arXiv preprint arXiv:2112.03126*, 2021.
- [9] Adrien Bardes, Quentin Garrido, Jean Ponce, Xinlei Chen, Michael Rabbat, Yann LeCun, Mahmoud Assran, and Nicolas Ballas. Revisiting feature prediction for learning visual representations from video. *arXiv preprint arXiv:2404.08471*, 2024.
- [10] Solon Barocas, Moritz Hardt, and Arvind Narayanan. *Fairness and machine learning: Limitations and opportunities*. MIT press, 2023.
- [11] Marc G Bellemare, Yavar Naddaf, Joel Veness, and Michael Bowling. The arcade learning environment: An evaluation platform for general agents. *Journal of artificial intelligence research*, 47:253–279, 2013.
- [12] Yoshua Bengio, Nicholas Léonard, and Aaron Courville. Estimating or propagating gradients through stochastic neurons for conditional computation. *arXiv preprint arXiv:1308.3432*, 2013.
- [13] Mathilde Caron, Hugo Touvron, Ishan Misra, Hervé Jégou, Julien Mairal, Piotr Bojanowski, and Armand Joulin. Emerging properties in self-supervised vision transformers. In *Proceedings of the IEEE/CVF international conference on computer vision*, pages 9650–9660, 2021.
- [14] Chang Chen, Yi-Fu Wu, Jaesik Yoon, and Sungjin Ahn. Transdreamer: Reinforcement learning with transformer world models. *arXiv preprint arXiv:2202.09481*, 2022.
- [15] Ricky TQ Chen, Yulia Rubanova, Jesse Bettencourt, and David K Duvenaud. Neural ordinary differential equations. *Advances in neural information processing systems*, 31, 2018.
- [16] Cheng Chi, Siyuan Feng, Yilun Du, Zhenjia Xu, Eric Cousineau, Benjamin Burchfiel, and Shuran Song. Diffusion policy: Visuomotor policy learning via action diffusion. *arXiv preprint arXiv:2303.04137*, 2023.
- [17] Prafulla Dhariwal and Alexander Nichol. Diffusion models beat gans on image synthesis. *Advances in neural information processing systems*, 34:8780–8794, 2021.

- [18] Jeffrey L. Elman. Finding structure in time. *Cognitive Science*, 14(2):179–211, 1990.
- [19] Patrick Esser, Sumith Kulal, Andreas Blattmann, Rahim Entezari, Jonas Müller, Harry Saini, Yam Levi, Dominik Lorenz, Axel Sauer, Frederic Boesel, et al. Scaling rectified flow transformers for high-resolution image synthesis. In *Forty-first International Conference on Machine Learning*, 2024.
- [20] Karl Friston. The free-energy principle: a unified brain theory? *Nature reviews neuroscience*, 11(2):127–138, 2010.
- [21] Karl Friston, James Kilner, and Lee Harrison. A free energy principle for the brain. *Journal of physiology-Paris*, 100(1-3):70–87, 2006.
- [22] Jean-Bastien Grill, Florian Strub, Florent Altché, Corentin Tallec, Pierre Richemond, Elena Buchatskaya, Carl Doersch, Bernardo Avila Pires, Zhaohan Guo, Mohammad Gheshlaghi Azar, et al. Bootstrap your own latent-a new approach to self-supervised learning. *Advances in neural information processing systems*, 33:21271–21284, 2020.
- [23] Jean-Bastien Grill, Florian Strub, Florent Altché, Corentin Tallec, Pierre Richemond, Elena Buchatskaya, Carl Doersch, Bernardo Avila Pires, Zhaohan Guo, Mohammad Gheshlaghi Azar, et al. Bootstrap your own latent-a new approach to self-supervised learning. *Advances in neural information processing systems*, 33:21271–21284, 2020.
- [24] Suna Sihang Guo, Ruohan Zhang, Bo Liu, Yifeng Zhu, Dana Ballard, Mary Hayhoe, and Peter Stone. Machine versus human attention in deep reinforcement learning tasks. *Advances in neural information processing systems*, 34:25370–25385, 2021.
- [25] David Ha and Jürgen Schmidhuber. World models. *arXiv preprint arXiv:1803.10122*, 2018.
- [26] Danijar Hafner, Timothy Lillicrap, Ian Fischer, Ruben Villegas, David Ha, Honglak Lee, and James Davidson. Learning latent dynamics for planning from pixels. In *International conference on machine learning*, pages 2555–2565. PMLR, 2019.
- [27] Danijar Hafner, Timothy Lillicrap, Jimmy Ba, and Mohammad Norouzi. Dream to control: Learning behaviors by latent imagination. In *International Conference on Learning Representations*, 2020. URL <https://openreview.net/forum?id=S1l0TC4tDS>.
- [28] Danijar Hafner, Timothy Lillicrap, Mohammad Norouzi, and Jimmy Ba. Mastering atari with discrete world models. *arXiv preprint arXiv:2010.02193*, 2020.
- [29] Danijar Hafner, Jurgis Pasukonis, Jimmy Ba, and Timothy Lillicrap. Mastering diverse domains through world models. *arXiv preprint arXiv:2301.04104*, 2023.
- [30] Nicklas Hansen, Xiaolong Wang, and Hao Su. Temporal difference learning for model predictive control. *arXiv preprint arXiv:2203.04955*, 2022.
- [31] Nicklas Hansen, Hao Su, and Xiaolong Wang. Td-mpc2: Scalable, robust world models for continuous control. *arXiv preprint arXiv:2310.16828*, 2023.
- [32] Moritz Hardt, Eric Price, and Nati Srebro. Equality of opportunity in supervised learning. *Advances in neural information processing systems*, 29, 2016.
- [33] Jonathan Ho and Tim Salimans. Classifier-free diffusion guidance. *arXiv preprint arXiv:2207.12598*, 2022.
- [34] Jonathan Ho, Ajay Jain, and Pieter Abbeel. Denoising diffusion probabilistic models. *Advances in neural information processing systems*, 33:6840–6851, 2020.
- [35] Sepp Hochreiter and Jürgen Schmidhuber. Long short-term memory. *Neural Computation*, 9(8):1735–1780, 1997. doi: 10.1162/neco.1997.9.8.1735.
- [36] Michael Janner, Yilun Du, Joshua B Tenenbaum, and Sergey Levine. Planning with diffusion for flexible behavior synthesis. *arXiv preprint arXiv:2205.09991*, 2022.

- [37] Leslie Pack Kaelbling, Michael L Littman, and Anthony R Cassandra. Planning and acting in partially observable stochastic domains. *Artificial intelligence*, 101(1-2):99–134, 1998.
- [38] Lukasz Kaiser, Mohammad Babaeizadeh, Piotr Milos, Blazej Osinski, Roy H Campbell, Konrad Czechowski, Dumitru Erhan, Chelsea Finn, Piotr Kozakowski, Sergey Levine, et al. Model-based reinforcement learning for atari. *arXiv preprint arXiv:1903.00374*, 2019.
- [39] Tero Karras, Miika Aittala, Timo Aila, and Samuli Laine. Elucidating the design space of diffusion-based generative models. *Advances in neural information processing systems*, 35: 26565–26577, 2022.
- [40] Diederik P Kingma and Max Welling. Auto-encoding variational bayes. *arXiv preprint arXiv:1312.6114*, 2013.
- [41] Yann LeCun. A path towards autonomous machine intelligence version 0.9. 2, 2022-06-27. *Open Review*, 62(1):1–62, 2022.
- [42] Yaron Lipman, Ricky TQ Chen, Heli Ben-Hamu, Maximilian Nickel, and Matt Le. Flow matching for generative modeling. *arXiv preprint arXiv:2210.02747*, 2022.
- [43] Songming Liu, Lingxuan Wu, Bangguo Li, Hengkai Tan, Huayu Chen, Zhengyi Wang, Ke Xu, Hang Su, and Jun Zhu. Rdt-1b: a diffusion foundation model for bimanual manipulation. *arXiv preprint arXiv:2410.07864*, 2024.
- [44] Yixin Liu, Kai Zhang, Yuan Li, Zhiling Yan, Chujie Gao, Ruoxi Chen, Zhengqing Yuan, Yue Huang, Hanchi Sun, Jianfeng Gao, et al. Sora: A review on background, technology, limitations, and opportunities of large vision models. *arXiv preprint arXiv:2402.17177*, 2024.
- [45] Grace Luo, Lisa Dunlap, Dong Huk Park, Aleksander Holynski, and Trevor Darrell. Diffusion hyperfeatures: Searching through time and space for semantic correspondence. *Advances in Neural Information Processing Systems*, 36:47500–47510, 2023.
- [46] Yunhao Luo, Chen Sun, Joshua B Tenenbaum, and Yilun Du. Potential based diffusion motion planning. *arXiv preprint arXiv:2407.06169*, 2024.
- [47] Yi Ma, Doris Tsao, and Heung-Yeung Shum. On the principles of parsimony and self-consistency for the emergence of intelligence. *Frontiers of Information Technology & Electronic Engineering*, 23(9):1298–1323, 2022.
- [48] Vincent Micheli, Eloi Alonso, and François Fleuret. Transformers are sample-efficient world models. *arXiv preprint arXiv:2209.00588*, 2022.
- [49] Vincent Micheli, Eloi Alonso, and François Fleuret. Transformers are sample-efficient world models. In *The Eleventh International Conference on Learning Representations*, 2023. URL <https://openreview.net/forum?id=vhFu1Acb0xb>.
- [50] Volodymyr Mnih, Koray Kavukcuoglu, David Silver, Andrei A Rusu, Joel Veness, Marc G Bellemare, Alex Graves, Martin Riedmiller, Andreas K Fidjeland, Georg Ostrovski, et al. Human-level control through deep reinforcement learning. *nature*, 518(7540):529–533, 2015.
- [51] Hans Moravec. *Mind children: The future of robot and human intelligence*. Harvard University Press, 1988.
- [52] Allen Newell. Intellectual issues in the history of artificial intelligence. *Artificial Intelligence: Critical Concepts*, pages 25–70, 1982.
- [53] Beatrix MG Nielsen, Anders Christensen, Andrea Dittadi, and Ole Winther. Diffenc: Variational diffusion with a learned encoder. *arXiv preprint arXiv:2310.19789*, 2023.
- [54] Kushagra Pandey, Avideep Mukherjee, Piyush Rai, and Abhishek Kumar. Diffusevae: Efficient, controllable and high-fidelity generation from low-dimensional latents. *arXiv preprint arXiv:2201.00308*, 2022.

- [55] Jack Parker-Holder, Stephen Spencer, Philip Ball, Jake Bruce, Vibhavari Dasagi, Kristian Holsheimer, Christos Kaplanis, Alexandre Moufarek, Guy Scully, Jeremy Shar, Jimmy Shi, Jessica Yung, Michael Dennis, Sultan Kenjeyev, Shangbang Long, Vlad Mnih, Harris Chan, Maxime Gazeau, Bonnie Li, Fabio Pardo, Luyu Wang, Lei Zhang, Frederic Besse, Tim Harley, Anna Mitenkova, Jane X. Wang, Jeff Clune, Demis Hassabis, Raia Hadsell, Adrian Bolton, Satinder Singh, and Tim Rocktäschel. Genie-2: A large-scale foundation world model. <https://deepmind.google/discover/blog/genie-2-a-large-scale-foundation-world-model/>, December 2024. Google DeepMind Blog.
- [56] Tobias Pohlen, Bilal Piot, Todd Hester, Mohammad Gheshlaghi Azar, Dan Horgan, David Budden, Gabriel Barth-Maron, Hado Van Hasselt, John Quan, Mel Večerík, et al. Observe and look further: Achieving consistent performance on atari. *arXiv preprint arXiv:1805.11593*, 2018.
- [57] Konpat Preechakul, Nattanat Chatthee, Suttisak Wizadwongsa, and Supasorn Suwajanakorn. Diffusion autoencoders: Toward a meaningful and decodable representation. In *Proceedings of the IEEE/CVF conference on computer vision and pattern recognition*, pages 10619–10629, 2022.
- [58] Danilo Rezende and Shakir Mohamed. Variational inference with normalizing flows. In *International conference on machine learning*, pages 1530–1538. PMLR, 2015.
- [59] Jan Robine, Marc Höftmann, Tobias Uelwer, and Stefan Harmeling. Transformer-based world models are happy with 100k interactions. *arXiv preprint arXiv:2303.07109*, 2023.
- [60] Robin Rombach, Andreas Blattmann, Dominik Lorenz, Patrick Esser, and Björn Ommer. High-resolution image synthesis with latent diffusion models. In *Proceedings of the IEEE/CVF conference on computer vision and pattern recognition*, pages 10684–10695, 2022.
- [61] Olaf Ronneberger, Philipp Fischer, and Thomas Brox. U-net: Convolutional networks for biomedical image segmentation. In *Medical image computing and computer-assisted intervention—MICCAI 2015: 18th international conference, Munich, Germany, October 5-9, 2015, proceedings, part III 18*, pages 234–241. Springer, 2015.
- [62] Alexander Shmakov, Kevin Greif, Michael Fenton, Aishik Ghosh, Pierre Baldi, and Daniel Whiteson. End-to-end latent variational diffusion models for inverse problems in high energy physics. *Advances in Neural Information Processing Systems*, 36:65102–65127, 2023.
- [63] David Silver, Aja Huang, Chris J Maddison, Arthur Guez, Laurent Sifre, George Van Den Driessche, Julian Schrittwieser, Ioannis Antonoglou, Veda Panneershelvam, Marc Lanctot, et al. Mastering the game of go with deep neural networks and tree search. *nature*, 529(7587):484–489, 2016.
- [64] David Silver, Thomas Hubert, Julian Schrittwieser, Ioannis Antonoglou, Matthew Lai, Arthur Guez, Marc Lanctot, Laurent Sifre, Dhharshan Kumaran, Thore Graepel, et al. Mastering chess and shogi by self-play with a general reinforcement learning algorithm. *arXiv preprint arXiv:1712.01815*, 2017.
- [65] Joar Skalse, Nikolaus Howe, Dmitrii Krasheninnikov, and David Krueger. Defining and characterizing reward gaming. *Advances in Neural Information Processing Systems*, 35:9460–9471, 2022.
- [66] Jascha Sohl-Dickstein, Eric Weiss, Niru Maheswaranathan, and Surya Ganguli. Deep unsupervised learning using nonequilibrium thermodynamics. In *International conference on machine learning*, pages 2256–2265. PMLR, 2015.
- [67] Yang Song and Stefano Ermon. Generative modeling by estimating gradients of the data distribution. *Advances in neural information processing systems*, 32, 2019.
- [68] Yang Song, Jascha Sohl-Dickstein, Diederik P Kingma, Abhishek Kumar, Stefano Ermon, and Ben Poole. Score-based generative modeling through stochastic differential equations. *arXiv preprint arXiv:2011.13456*, 2020.

- [69] Richard S Sutton. Learning to predict by the methods of temporal differences. *Machine learning*, 3:9–44, 1988.
- [70] Richard S Sutton. Dyna, an integrated architecture for learning, planning, and reacting. *ACM Sigart Bulletin*, 2(4):160–163, 1991.
- [71] Yuval Tassa, Yotam Doron, Alistair Muldal, Tom Erez, Yazhe Li, Diego de Las Casas, David Budden, Abbas Abdolmaleki, Josh Merel, Andrew Lefrancq, Timothy Lillicrap, and Martin Riedmiller. Deepmind control suite, 2018. URL <https://arxiv.org/abs/1801.00690>.
- [72] Zhendong Wang, Jonathan J Hunt, and Mingyuan Zhou. Diffusion policies as an expressive policy class for offline reinforcement learning. *arXiv preprint arXiv:2208.06193*, 2022.
- [73] Zixin Wen and Yuanzhi Li. The mechanism of prediction head in non-contrastive self-supervised learning. *Advances in Neural Information Processing Systems*, 35:24794–24809, 2022.
- [74] Ronald J Williams. Simple statistical gradient-following algorithms for connectionist reinforcement learning. *Machine learning*, 8:229–256, 1992.
- [75] Philipp Wu, Alejandro Escontrela, Danijar Hafner, Pieter Abbeel, and Ken Goldberg. Daydreamer: World models for physical robot learning. In *Conference on robot learning*, pages 2226–2240. PMLR, 2023.
- [76] Weilai Xiang, Hongyu Yang, Di Huang, and Yunhong Wang. Denoising diffusion autoencoders are unified self-supervised learners. In *Proceedings of the IEEE/CVF International Conference on Computer Vision*, pages 15802–15812, 2023.
- [77] Xingyi Yang and Xinchao Wang. Diffusion model as representation learner. In *Proceedings of the IEEE/CVF International Conference on Computer Vision*, pages 18938–18949, 2023.
- [78] Zhongqi Yue, Jiankun Wang, Qianru Sun, Lei Ji, Eric I Chang, Hanwang Zhang, et al. Exploring diffusion time-steps for unsupervised representation learning. *arXiv preprint arXiv:2401.11430*, 2024.
- [79] Weipu Zhang, Gang Wang, Jian Sun, Yetian Yuan, and Gao Huang. Storm: Efficient stochastic transformer based world models for reinforcement learning. *Advances in Neural Information Processing Systems*, 36:27147–27166, 2023.
- [80] Zijian Zhang, Zhou Zhao, and Zhijie Lin. Unsupervised representation learning from pre-trained diffusion probabilistic models. *Advances in neural information processing systems*, 35: 22117–22130, 2022.

A Supplementary Background and Related Works

A.1 Score-based diffusion models and flow matching

Modern diffusion models can be generalized to a continuous score-based generative SDE which flows forward and backward from gaussian noise to data[5, 68]. At first glance, learning a neural network \mathbf{F}_θ for this resembles earlier works that require solving an ODE during training[15, 58]. However, the main novelty of diffusion models lies in the fact that simulation-free efficient and unbiased training can be achieved because a specific sample-conditional path was pre-determined. Surprisingly, the intractable objective of regressing $\mathbf{F}_\theta(\mathbf{z}, \tau)$ towards the marginal probability $\mathbf{p}(\mathbf{z})$ at diffusion time step τ :

$$\mathcal{L}(\theta) = \mathbb{E}_{\tau, z^0} [\|\mathbf{F}_\theta(\mathbf{z}^\tau, \tau) - \nabla_{\mathbf{z}^\tau} \log \mathbf{p}^\tau(\mathbf{z})\|^2] \quad (6)$$

has the same gradient as regressing towards the tractable sample-conditional vector field derived from our choice of probability path in expectation [3, 42]:

$$\mathcal{L}(\theta) = \mathbb{E}_{\tau, z^0} [\|\mathbf{F}_\theta(\mathbf{z}^\tau, \tau) - \nabla_{\mathbf{z}^\tau} \log \mathbf{p}^{0\tau}(\mathbf{z}^\tau | \mathbf{z}^0)\|^2] \quad (7)$$

where the expectation is over τ , and the noised sample $\mathbf{z} \sim \mathbf{p}^{0\tau}(\mathbf{z}^\tau | \mathbf{z}^0)$, depends on the pre-determined probability path conditional on clean samples $z^0 \sim p^0$. This can be derived from linear interpolation or the standard diffusion path at time step τ . With this, the second term for Eqn 7 becomes trivial.

Related works. Score-based generative models or diffusion models was first introduced in Noise Conditional Score Network (NCSN) [67]. Ho et al. [34] popularized this approach by drawing the link between NCSNs to Diffusion Models [66]. Karras et al. [39] elucidated design space of diffusion with neural networks and arrived at the ideal training framework, EDM, including network preconditioning. There are many efforts to build a high-fidelity world model with latent diffusion model which leverage on a pretrained encoder [60, 19, 44, 7, 55]. A separate line of work leverages diffusion models for planning directly on the observation space without any compression [36, 46]. [16, 72, 43] uses diffusion models for policy learning, with an image encoder learned end-to-end with the use of supervised learning. Works that explore diffusion models for representation learning use search through diffusion denoising inference outputs [45, 78], require distillation from a larger pretrained model [77, 80], involve using a pixel-based conditional diffusion model conditioned on compressed representation from an encoder trained through an augmented diffusion loss [57, 78, 1, 54, 53]. [8, 76] leverage the hidden activations of the diffusion network to find a suitable representation. Our work is the first to leverage a diffusion model for predicting compressed representations in an end-to-end fashion, without reconstruction and searching through denoising outputs or hidden activations. Shmakov et al. [62] learns an encoder and latent end-to-end diffusion model but it requires a decoder and the domain was in high energy physics. Our work is the first latent end-to-end diffusion model for learning and predicting compressed representations in a self-supervised manner, without reconstruction and searching through denoising outputs or hidden activations.

B Changes Compared to Baseline and Hyperparameters

We used the DIAMOND library [4] (MIT License) for our implementation. The main difference between JEDI World Model and DIAMOND is the transplant of the DIAMOND’s RL encoder onto the JEDI World Model and the techniques implemented to facilitate end-to-end latent diffusion mentioned in §4. The only network architectural changes are practical: (1) changing the original RL encoder to downsample to $z_t \in [-3, 3]^{16 \times 8 \times 8}$, (2) modifying the diffusion UNET [61] into a single layer without downsampling, (3) and removing the downsampling in the Reward/Termination Model’s encoder. The only hyperparameter changes were increasing the diffusion model’s warm-up learning steps to 1000 and sigma of input data to be 1.

B.1 JEDI Algorithm

Green font refers to changes as compared to pixel-based diffusion world model baseline [4]

Algorithm 1 JEDI Training

```
1: procedure TRAINING_LOOP
2:   for epochs do
3:     collect_experience(steps_collect)
4:     for steps_diffusion_model do
5:       update_latent_diffusion_model()
6:     end for
7:     for steps_reward_end_model do
8:       update_reward_end_model()
9:     end for
10:    for steps_actor_critic do
11:      update_actor_critic()
12:    end for
13:  end for
14: end procedure

15: procedure COLLECT_EXPERIENCE( $n$ )
16:    $x_0 \leftarrow \text{env.reset}()$ 
17:   for  $t = 0$  to  $n - 1$  do
18:     Sample  $a_t \sim \pi_\omega(a_t|z_t^0)q_\phi(z_t^0|x_t)$   $\triangleright$  derive  $z_t^0$  using JEDI encoder  $\mathbf{E}_\phi$  before sampling action
19:      $x_{t+1}, r_t, d_t \leftarrow \text{env.step}(a_t)$ 
20:      $\mathcal{D} \leftarrow \mathcal{D} \cup \{x_t, a_t, r_t, d_t\}$ 
21:     if  $d_t = \text{true}$  then
22:        $x_{t+1} \leftarrow \text{env.reset}()$ 
23:     end if
24:   end for
25: end procedure

26: procedure UPDATE_LATENT_DIFFUSION_MODEL
27:   Sample sequence  $(x_{t-L+1}, a_{t-L+1}, \dots, x_t, a_t, x_{t+1}) \sim \mathcal{D}$ 
28:   Sample  $\log(\sigma) \sim \mathcal{N}(P_{\text{mean}}, P_{\text{std}}^2)$   $\triangleright$  log-normal sigma distribution from EDM
29:   Define  $\tau := \sigma$   $\triangleright$  default identity schedule from EDM
30:   compute  $[z_{t-L+1}^0, \dots, z_t^0, z_{t+1}^0] = C(\mathbf{E}_\phi([x_{t-L+1}, \dots, x_t, x_{t+1}]))$   $\triangleright$  derive the clamped latents
31:   derive  $z_{t+1}^0 = \text{sg}(z_{t+1}^0)$   $\triangleright$  detach gradients from the target latent
32:   Sample  $z_{t+1}^{\tau} \sim \mathcal{N}(z_{t+1}^0, \sigma^2 \mathbf{I})$   $\triangleright$  add independent Gaussian noise
33:   Compute  $z_{t+1}^0 = \mathbf{D}_\theta(z_{t+1}^{\tau}, \tau, z_{t-L+1}^0, a_{t-L+1}, \dots, z_t^0, a_t)$ 
34:   Compute reconstruction loss  $\mathcal{L}(\theta) = \|\hat{z}_{t+1}^0 - z_{t+1}^0\|^2$ 
35:    $rs \sim \text{Uniform}\{\text{True}, \text{False}\}$ 
36:   if  $rs = \text{True}$  then  $\triangleright$  random switch between  $\hat{z}_{t+1}^0$  or  $z_{t+1}^0$  as  $\mathbf{D}_\theta$  input for loss at  $t + 1$ 
37:     Cache  $\hat{z}_{t+1}^0$  as input to  $\mathbf{D}_\theta$  for UPDATE_LATENT_DIFFUSION_MODEL at  $t + 1$ 
38:   end if
39:   Update  $\mathbf{D}_\theta$ 
40: end procedure

41: procedure UPDATE_REWARD_END_MODEL
42:   Sample indexes  $\mathcal{I} = \{t, \dots, t + L + H - 1\}$   $\triangleright$  burn-in + imagination horizon
43:   Sample sequence  $(x_i, a_i, r_i, d_i)_{i \in \mathcal{I}} \sim \mathcal{D}$ 
44:   Compute  $(z_i^0)_{i \in \mathcal{I}} = C(\mathbf{E}_\phi((x_i)_{i \in \mathcal{I}}))$   $\triangleright$  derive the clamped latents
45:   Initialize  $h = c = 0$   $\triangleright$  LSTM hidden and cell states
46:   for  $i \in \mathcal{I}$  do
47:     Compute  $\hat{r}_i, \hat{d}_i, h, c = R_\psi(z_i^0, a_i, h, c)$ 
48:   end for
49:   Compute  $\mathcal{L}(\psi) = \sum_{i \in \mathcal{I}} \text{CE}(\hat{r}_i, \text{sign}(r_i)) + \text{CE}(\hat{d}_i, d_i)$   $\triangleright$  CE: cross-entropy loss
50:   Update  $R_\psi$ 
51: end procedure

52: procedure UPDATE_ACTOR_CRITIC
53:   Sample initial buffer  $(x_{t-L+1}, a_{t-L+1}, \dots, x_t) \sim \mathcal{D}$ 
54:   Compute  $[z_{t-L+1}^0, \dots, z_t^0] = C(\mathbf{E}_\phi([x_{t-L+1}, \dots, x_t]))$   $\triangleright$  derive the clamped latents
55:   Burn-in buffer with  $R_\psi, \pi_\omega$  and  $V_\omega$  to initialize LSTM states
56:   for  $i = t$  to  $t + H - 1$  do
57:     Sample  $a_i \sim \pi_\omega(a_i|z_i^0)$ 
58:     Sample reward  $r_i$  and termination  $d_i$  with  $R_\psi$ 
59:     Sample next observation  $z_{i+1}^0$  by simulating reverse diffusion process with  $\mathbf{D}_\theta$ 
60:   end for
61:   Compute  $V_\omega(z_i^0)$  for  $i = t, \dots, t + H$ 
62:   Compute RL losses  $\mathcal{L}_V(\omega)$  and  $\mathcal{L}_\pi(\omega)$ 
63:   Update  $\pi_\omega$  and  $V_\omega$ 
64: end procedure
```

Table 3: Model architecture details for JEDI. Green font refers to changes as compared to pixel-based diffusion world model baseline [4]. Downsampling layers refers to the Maxpool operation that downsamples the input height and width by a factor of 2.

| Hyperparameter | Value |
|---|------------------------------|
| Latent Diffusion Dynamics Model (D_θ) | |
| State conditioning mechanism | Frame stacking |
| Action conditioning mechanism | Adaptive Group Normalization |
| Diffusion time conditioning mechanism | Adaptive Group Normalization |
| Residual blocks layers | [1] |
| Residual blocks channels | [160] |
| UNET Downsampling | NIL |
| Residual blocks conditioning dimension | 256 |
| Sigma data (for preconditioning) | 1 |
| World Model Encoder (E_ϕ) | |
| Encoder blocks layers | [1, 1, 1, 1] |
| Encoder blocks channels | [32, 32, 32, 16] |
| Encoder Downsampling layers | [1,1,1,0] |
| Encoder tanh clamp factor | 3 |
| Reward/Termination Model (R_ψ) | |
| Action conditioning mechanisms | Adaptive Group Normalization |
| Residual blocks layers | [2, 2, 2, 2] |
| Residual blocks channels | [32, 32, 32, 32] |
| Encoder Downsampling layers | NIL |
| Residual blocks conditioning dimension | 128 |
| LSTM dimension | 512 |
| Actor-Critic Model (π_ω and V_ω) | |
| Encoder | NIL |
| LSTM dimension | 512 |

Table 4: Training hyperparameters for JEDI. Green font refers to changes as compared to pixel-based diffusion world model baseline [4].

| Hyperparameter | Value |
|--|-------------------------------------|
| Training loop | |
| Number of epochs | 1000 |
| Training steps per epoch | 400 |
| Batch size | 32 |
| Environment steps per epoch | 100 |
| Epsilon (greedy) for collection | 0.01 |
| RL hyperparameters | |
| Imagination horizon (H) | 15 |
| Discount factor (γ) | 0.985 |
| Entropy weight (η) | 0.001 |
| λ -returns coefficient (λ) | 0.95 |
| Sequence construction during training | |
| For D_θ , number of conditioning observations and actions (L) | 4 |
| For R_ψ , burn-in length (B_R), set to L in practice | 4 |
| For R_ψ , training sequence length ($B_R + H$) | 19 |
| For π_ϕ and V_ϕ , burn-in length ($B_{\pi,V}$), set to L in practice | 4 |
| Optimization | |
| Optimizer | AdamW |
| Learning rate | 1e-4 |
| Epsilon | 1e-8 |
| Weight decay (D_θ) | 1e-2 |
| Weight decay (R_ψ) | 1e-2 |
| Weight decay (π_ϕ and V_ϕ) | 0 |
| Learning rate Warm-up steps (D_θ) | 1e3 |
| Learning rate Warm-up steps (R_ψ) | 1e2 |
| Learning rate Warm-up steps (π_ω and V_ω) | 1e2 |
| Learning rate scale factor for E_ϕ | 0.3 |
| Diffusion Sampling | |
| Method | Euler |
| Number of steps | 3 |
| S churn | 1 (only for stochastic experiments) |
| Environment | |
| Image observation dimensions | $64 \times 64 \times 3$ |
| Action space | Discrete (up to 18 actions) |
| Frameskip | 4 |
| Frameskip for Stochastic Experiments | [2, 6] |
| Max noop | 30 |
| Termination on life loss | True |
| Reward clipping | {-1, 0, 1} |

C Supplementary Results

C.1 Derivation of STORM’s results

As we are limited by our computational budget, we were unable to run the baseline by Zhang et al. [79] (STORM) and thus unable to derive their seed level performance as it is not publicly available. As such, we were unable to derive any metrics that are not available in pre-existing literature. For the Human Normalized Score aggregates on the overall Atari100k, we obtained STORM’s Mean and Median from its main paper [79] and we obtained its Interquartile mean from Alonso et al. [4]. The STORM error bars in Figure 4 were visually recreated from the error bars presented in Alonso et al. [4]. For other aggregates on different configurations of Atari100k e.g. Agent Normalized Scores and Human Normalized Scores on Agent-Optimal and Human-Optimal tasks, we are only able to derive the point estimate for the Mean.

Table 5: Atari100k overall performance. Blue font and red font refers to outperforming and underperforming to DIAMOND respectively. The tasks are sorted in decreasing HNS of the averaged agent level performance (§5.1). Middle line indicates the split between the Agent-Optimal and Human-Optimal tasks respectively. Bold refers to the best result, underline refers to the runner-up. DIAMD = DIAMOND, DrmrV3 = DreamerV3. JEDI achieves SOTA optimality gap and runner-up performance in number of super-human games achieved and overall mean.

| Game | Random | Human | SimPLE | TWM | IRIS | DrmrV3 | STORM | DIAMD | JEDI |
|--------------------|---------|----------------|---------|----------------|---------------|--------------|----------------|----------------|---------------|
| Boxing | 0.1 | 12.1 | 7.8 | 77.5 | 70.1 | 73.8 | 79.7 | 86.9 | 93.8 |
| Krull | 1598.0 | 2665.5 | 2204.8 | 6349.2 | 6616.4 | 7921.5 | 8412.6 | 8610.1 | 8844.4 |
| CrazyClimber | 10780.5 | 35829.4 | 62583.6 | 71820.4 | 59324.2 | 84880.0 | 66776.0 | 99167.8 | 56614.3 |
| Gopher | 257.6 | 2412.5 | 596.8 | 1674.8 | 2236.1 | 5754.3 | 8239.6 | 5897.9 | 4026.9 |
| RoadRunner | 11.5 | 7845.0 | 5640.6 | 9109.0 | 9614.6 | 14995.0 | 17564.0 | 20673.2 | 14520.3 |
| Jamesbond | 29.0 | 302.8 | 100.5 | 362.4 | 462.7 | 480.4 | 509.0 | 427.4 | 455.8 |
| Assault | 222.4 | 742.0 | 527.2 | 682.6 | 1524.4 | 669.7 | 801.0 | 1526.4 | 1591.1 |
| Breakout | 1.7 | 30.5 | 16.4 | 20.0 | 83.7 | 27.9 | 15.9 | 132.5 | 159.3 |
| KungFuMaster | 258.5 | 22736.3 | 14862.5 | 24554.6 | 21759.8 | 24210.0 | 26182.0 | 18713.6 | 11632.7 |
| Pong | -20.7 | 14.6 | 12.8 | 18.8 | 14.6 | 18.9 | 11.3 | 20.4 | 17.6 |
| Kangaroo | 52.0 | 3035.0 | 51.2 | 1240.0 | 838.2 | 3790.0 | 4208.0 | 5382.2 | 980.0 |
| UpNDown | 533.4 | 11693.2 | 3350.3 | 15981.7 | 3546.2 | 7981.7 | 7985.0 | 3856.3 | 3889.0 |
| Freeway | 0.0 | 29.6 | 16.7 | 24.3 | 31.1 | 0.0 | 33.5 | 33.3 | 6.7 |
| BankHeist | 14.2 | 753.1 | 34.2 | 466.7 | 53.1 | 622.7 | 641.2 | 19.7 | 1021.8 |
| DemonAttack | 152.1 | 1971.0 | 208.1 | 350.2 | 2034.4 | 433.7 | 164.6 | 288.1 | 1724.6 |
| Hero | 1027.0 | 30826.4 | 2656.6 | 7254.0 | 7037.4 | 11145.2 | 11044.3 | 5621.8 | 5908.6 |
| BattleZone | 2360.0 | 37187.5 | 4031.2 | 5068.0 | 13074.0 | 12400.0 | 13540.0 | 4702.0 | 18763.3 |
| Frostbite | 65.2 | 4334.7 | 236.9 | 1475.6 | 259.1 | 945.1 | 1316.0 | 274.1 | 255.8 |
| Qbert | 163.9 | 13455.0 | 1288.8 | 3330.8 | 745.7 | 3291.3 | 4522.5 | 4499.3 | 3562.0 |
| MsPacman | 307.3 | 6951.6 | 1480.0 | 1588.4 | 999.1 | 1358.4 | 2673.5 | 1958.2 | 1004.0 |
| Asterix | 210.0 | 8503.3 | 1128.3 | 1116.6 | 853.6 | 946.4 | 1028.0 | 3698.5 | 2110.0 |
| ChopperCommand | 811.0 | 7387.8 | 979.4 | 1697.4 | 1565.0 | 411.7 | 1888.0 | 1369.8 | 1331.3 |
| Amidar | 5.8 | 1719.5 | 74.3 | 121.8 | 143.0 | 141.2 | 204.8 | 225.8 | 122.3 |
| Alien | 227.8 | 7127.7 | 616.9 | 674.6 | 420.0 | 1078.9 | 983.6 | 744.1 | 1377.1 |
| PrivateEye | 24.9 | 69571.3 | 35.0 | 86.6 | 100.0 | 1081.4 | 7781.0 | 114.3 | 92.0 |
| Seaquest | 68.4 | 42054.7 | 683.3 | 774.4 | 661.3 | 610.0 | 525.2 | 551.2 | 1085.1 |
| #Superhuman (↑) | 0 | N/A | 1 | 8 | <u>10</u> | 9 | <u>10</u> | 11 | <u>10</u> |
| Mean (↑) | 0.000 | 1.000 | 0.332 | 0.956 | 1.046 | 1.134 | 1.266 | 1.459 | <u>1.383</u> |
| Median (↑) | 0.000 | 1.000 | 0.134 | <u>0.505</u> | 0.289 | 0.503 | 0.584 | 0.373 | 0.391 |
| IQM (↑) | N/A | N/A | 0.130 | 0.459 | 0.501 | 0.504 | <u>0.636</u> | 0.641 | 0.594 |
| Optimality Gap (↓) | N/A | N/A | 0.729 | 0.513 | 0.512 | <u>0.500</u> | NA | 0.480 | 0.480 |

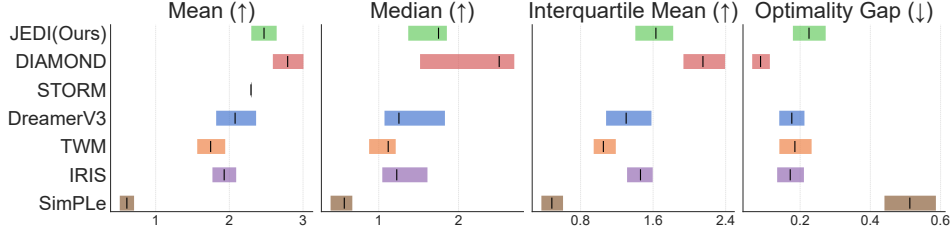


Figure 9: **Human Normalized Score** aggregates on the **Agent-Optimal** Atari100k games. Optimality Gap (\downarrow) is the overall gap to human-level performance. JEDI achieves runner-up performance in Mean, Median and Interquartile Mean.

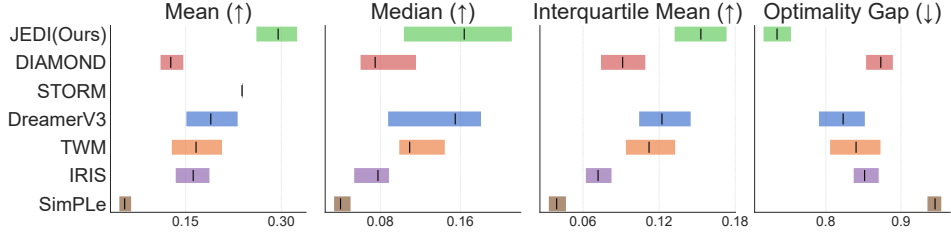


Figure 10: **Human Normalized Score** aggregates on the **Human-Optimal** Atari100k games. Optimality Gap (\downarrow) is the overall gap to human-level performance. JEDI achieves SOTA in Mean, Median, Interquartile Mean and Optimality Gap.

C.2 Raw scores for agent-level performance

The agent-level performance we used as reference to derive the Agent-Optimal tasks and Human-Optimal tasks was derived from the averaged raw scores of the 4 baselines [59, 48, 29, 79] selected in §5.1. Below is the agent-level performance raw score for each game. With the raw scores for

| Agent-Optimal Tasks | Raw Scores | Human-Optimal Tasks | Raw Scores |
|---------------------|------------|-----------------------|------------|
| <i>Boxing</i> | 76.325 | <i>BankHeist</i> | 452.5 |
| <i>Krull</i> | 7290.05 | <i>DemonAttack</i> | 713.05 |
| <i>CrazyClimber</i> | 73777.65 | <i>Hero</i> | 9124.175 |
| <i>Gopher</i> | 3970.125 | <i>BattleZone</i> | 10983 |
| <i>RoadRunner</i> | 12963.15 | <i>Frostbite</i> | 989.925 |
| <i>Jamesbond</i> | 444.775 | <i>Qbert</i> | 3001 |
| <i>Assault</i> | 928.5 | <i>MsPacman</i> | 1647 |
| <i>Breakout</i> | 37.65 | <i>Asterix</i> | 982.55 |
| <i>KungFuMaster</i> | 23479.1 | <i>ChopperCommand</i> | 1392.6 |
| <i>Pong</i> | 15.675 | <i>Amidar</i> | 152.15 |
| <i>Kangaroo</i> | 2596.05 | <i>Alien</i> | 759.3 |
| <i>UpNDown</i> | 9186.725 | <i>PrivateEye</i> | 2212.4 |
| <i>Freeway</i> | 22.225 | <i>Seaquest</i> | 644.725 |

Table 6: Raw scores for agent-level performance.

agent-level performance, we can derive the same aggregates for the Overall, Agent-Optimal and Human-Optimal Atari100k tasks, as shown in Figure 11 12 13. With respect to Agent Normalized Scores, JEDI achieves competitive performance on Overall and Agent-Optimal tasks, and achieves SOTA performance on all Human-Optimal tasks metrics except for Mean, where it achieved runner-up performance.

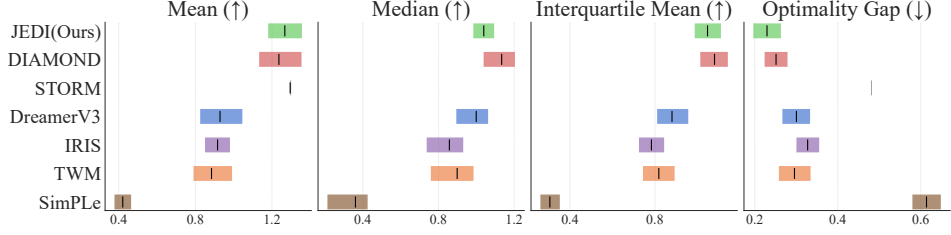


Figure 11: **Agent Normalized Score** Aggregates on the **Overall** Atari100k tasks. Optimality Gap (↓) is the overall gap to agent-level performance. Agent-level raw scores derived in appendix C.2. JEDI achieves SOTA Optimality Gap and runner-up performance in Mean, Median and Interquartile Mean.

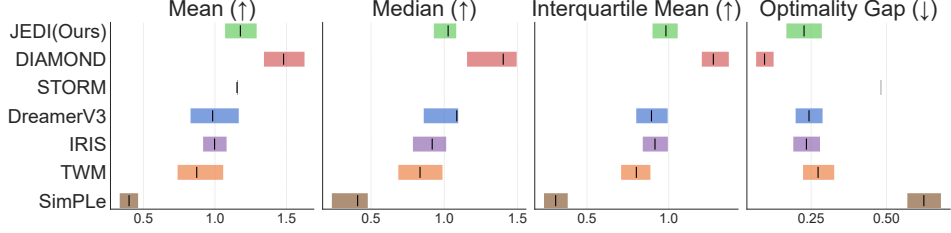


Figure 12: **Agent Normalized Score** Aggregates on the **Agent-Optimal** Atari100k tasks. Optimality Gap (↓) is the overall gap to agent-level performance. Agent-level raw scores derived in appendix C.2. JEDI achieves runner-up performance in Mean, Interquartile Mean and Optimality Gap.

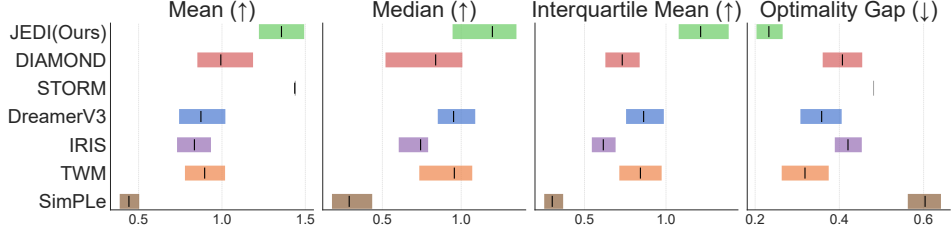


Figure 13: **Agent Normalized Score** Aggregates on the **Human-Optimal** Atari100k tasks. Optimality Gap (↓) is the overall gap to agent-level performance. Agent-level raw scores derived in appendix C.2. JEDI achieves SOTA Median, Interquartile Mean and Optimality Gap and runner-up performance on Mean.

Table 7: Relative Atari100k performance of all methods against DIAMOND. Check marks and cross marks refers to outperforming and underperforming to DIAMOND respectively. Bold font indicates the best results and underline indicates the runner-up. Pre-existing baselines’ outperformance against DIAMOND is biased towards the Human-Optimal set. JEDI is able to outperform DIAMOND in a more holistic fashion across both Agent-Optimal and Human-Optimal games.

| Agent-Optimal | IRIS | TWM | DrmrV3 | STORM | DIAMOND | JEDI | Human-Optimal | IRIS | TWM | DrmrV3 | STORM | DIAMOND | JEDI |
|--------------------|--------------|-------|--------|-------|----------------|--------------|--------------------|----------|--------------|--------------|-------|---------------|--------------|
| Boxing | × | × | × | × | 86.9 | ✓ | BankHeist | ✓ | ✓ | ✓ | ✓ | 19.7 | ✓ |
| Krull | × | × | × | × | 8610.1 | ✓ | DemonAttack | ✓ | ✓ | ✓ | × | 288.1 | ✓ |
| CrazyClimber | × | × | × | × | 99167.8 | × | Hero | ✓ | ✓ | ✓ | ✓ | 5621.8 | ✓ |
| Gopher | × | × | × | ✓ | 5897.9 | × | BattleZone | ✓ | ✓ | ✓ | ✓ | 4702.0 | ✓ |
| RoadRunner | × | × | × | × | 20673.2 | × | Frostbite | × | ✓ | ✓ | ✓ | 274.1 | × |
| Jamesbond | ✓ | × | ✓ | ✓ | 427.4 | ✓ | Qbert | × | × | × | ✓ | 4499.3 | × |
| Assault | × | × | × | × | 1526.4 | ✓ | MsPacman | × | × | × | ✓ | 1958.2 | × |
| Breakout | × | × | × | × | 132.5 | ✓ | Asterix | × | × | × | × | 3698.5 | × |
| KungFuMaster | ✓ | ✓ | ✓ | ✓ | 18713.6 | × | ChopperCommand | ✓ | ✓ | × | ✓ | 1369.8 | × |
| Pong | × | × | × | × | 20.4 | × | Amidar | × | × | × | × | 225.8 | × |
| Kangaroo | × | × | × | × | 5382.2 | × | Alien | × | × | ✓ | ✓ | 744.1 | ✓ |
| UpNDown | × | ✓ | ✓ | ✓ | 3856.3 | × | PrivateEye | × | × | ✓ | ✓ | 114.3 | × |
| Freeway | × | × | × | ✓ | 33.3 | × | Seaquest | ✓ | ✓ | ✓ | × | 551.2 | ✓ |
| #Superhuman (↑) | 9 | 8 | 9 | 10 | 11 | 9 | #Superhuman (↑) | 1 | 0 | 0 | 0 | 0 | 1 |
| Mean (↑) | 1.930 | 1.746 | 2.071 | 2.293 | 2.791 | <u>2.470</u> | Mean (↑) | 0.162 | 0.166 | <u>0.184</u> | 0.162 | 0.127 | 0.295 |
| Median (↑) | 1.226 | 1.119 | 1.356 | N/A | 2.510 | <u>1.749</u> | Median (↑) | 0.078 | <u>0.109</u> | 0.106 | N/A | 0.075 | 0.164 |
| IQM (↑) | 1.461 | 1.051 | 1.303 | N/A | 2.150 | <u>1.631</u> | IQM (↑) | 0.072 | 0.112 | <u>0.122</u> | N/A | 0.091 | 0.153 |
| Optimality Gap (↓) | <u>0.172</u> | 0.185 | 0.176 | N/A | 0.087 | 0.225 | Optimality Gap (↓) | 0.852 | 0.840 | <u>0.823</u> | N/A | 0.873 | 0.735 |

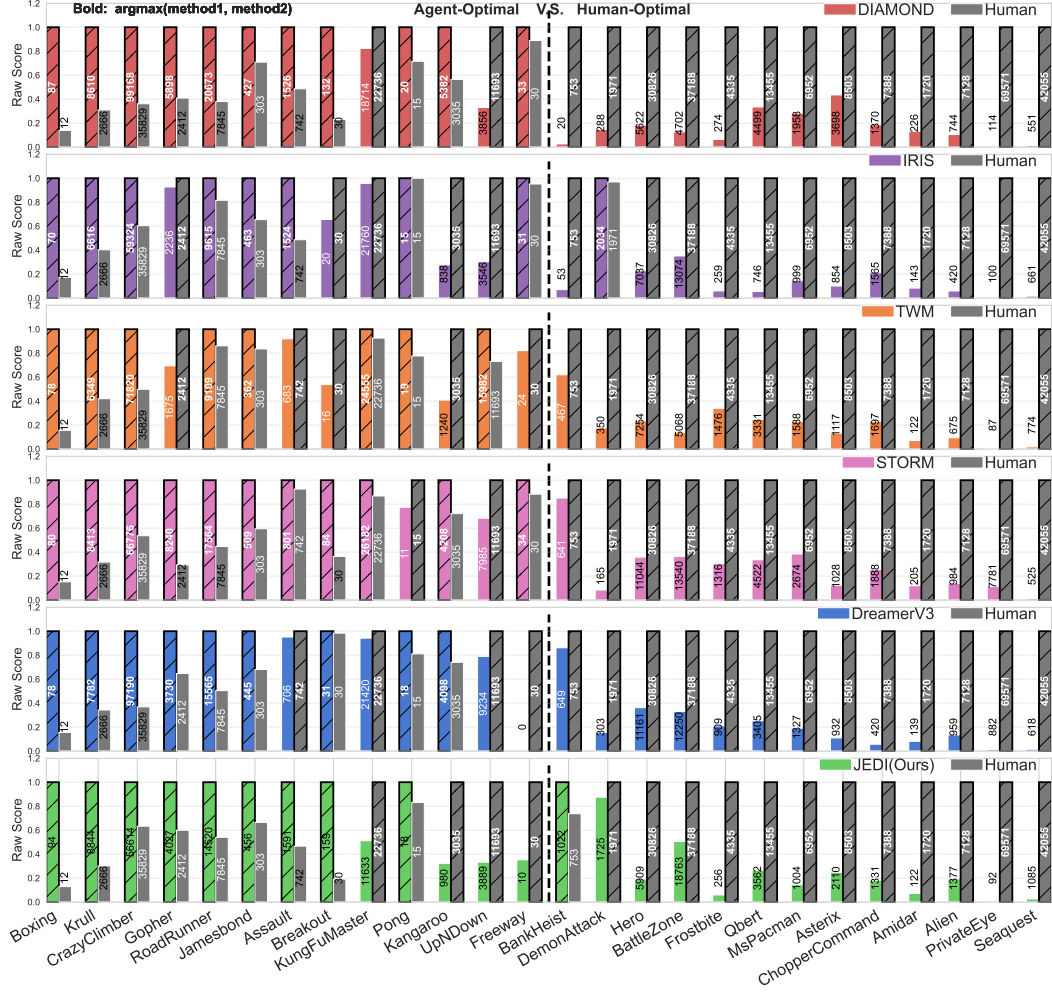


Figure 14: Performance asymmetry in MBRL algorithms in general. Bar heights are normalized by the max over the method and human score for every game. Bold refers to the argmax over the method and human score. It is clear that MBRL agents in general performs overwhelmingly well on the Agent-Optimal set while drastically performing worse in the Human-Optimal set. This is especially pronounced in pixel-based agents like DIAMOND and IRIS. JEDI mitigates this performance asymmetry with better performance in the Human-Optimal set.